Journal of The Electrochemical Society

The Electrochemical Society
Advancing solid state & electrochemical science & technology

ACCEPTED MANUSCRIPT

Mechanistic Analysis of Lithium-Air Battery with Organic Redox Mediator-Coated Air-Electrode

To cite this article before publication: Shota Azuma *et al* 2024 *J. Electrochem. Soc.* in press https://doi.org/10.1149/1945-7111/ad7f92

Mechanistic Analysis of Lithium-Air Battery with Organic Redox Mediator-Coated Air-Electrode

Journal:	*Journal of The Electrochemical Society*
Manuscript ID	JES-112969.R1
Manuscript Type:	Research Paper
Date Submitted by the Author:	09-Sep-2024
Complete List of Authors:	Azuma, Shota; National Institute for Materials Science; Seikei University Moro, Itsuki; Seikei University Sano, Mitsuki; Seikei University Ozawa, Fumisato; Seikei University, Department of Science and Technology Saito, Morihiro; Seikei University, Department of Materials and Life Science Nomura, Akihiro; National Institute for Materials Science
Keywords:	Batteries - Lithium, Energy Storage, Batteries

Mechanistic Analysis of Lithium-Air Battery with Organic Redox Mediator-Coated Air-Electrode

Shota Azuma,[1,2] Itsuki Moro,[1] Mitsuki. Sano,[1] Fumisato. Ozawa,[1] Morihiro Saito,[1,z] and Akihiro Nomura[2,z]

[1]Department of Materials and Life Science, Faculty of Science and Technology, Seikei University, Musashino-shi, Tokyo 180–8633, Japan

[2]Research Center for Energy and Environmental Materials, National Institute for Materials Science, Tsukuba, Ibaraki 305–0044, Japan

[z]E-mail: mosaito@st.seikei.ac.jp; NOMURA.Akihiro@nims.go.jp

Abstract

Redox mediators (RMs) suppress the charging overpotential to enhance the cycle performance of lithium-air batteries (LABs), but inappropriate RM incorporation can adversely shorten cycle life. In this study, three typical organic RMs; tetrathiafulvalene (TTF), 2,2,6,6-tetramethylpiperidine 1-oxyl (TEMPO), and 10-methylphenothiazine (MPT), were incorporated into the air-electrode (AE) of the LAB (RM-on-AE), rather than dissolving them in the electrolyte (RM-in-EL), to maximize the RM effect throughout the cycle life. The discharge/charge cycle test confirmed that the cells with RM-on-AE prevented the reductive decomposition of RM with the lithium anode, deriving the RM effect for a longer cycle life than the cells with RM-in-EL. The measurement of AE deposits revealed that the TTF- and TEMPO-on-AE cells failed to generate a quantitative amount of Li_2O_2 discharge product. In contrast, the MPT-on-AE provided a 96% yield of Li_2O_2 after the first discharge because of the reductive tolerance of the MPT as organic RM. The quantitative analysis also revealed an accumulation of Li_2CO_3 on the AEs, along with the generation of carboxylate, as the side products of irrelevant battery reactions. This study provides a practical methodology for selecting RMs and their incorporation for developing long-life LABs.

Introduction

Lithium-air batteries (LABs) have attracted attention because of their highest theoretical energy density (3500 Wh kg^{-1}, including oxygen mass) among the possible electrochemical storages [1]. Tremendous effort has been made to extend the lifetime of discharge/charge cycles to achieve rechargeable LAB cells with ultra-high energy density. However, it is still challenging to satisfy the practical requirements. Among the LAB materials, the air-electrode (AE) is crucial to battery performance, such as cell capacity and rate capability, proceeding the oxygen reduction/evolution reactions of LAB (ORR/OER, $2Li^+ + 2e^- + O_2 \rightarrow Li_2O_2$) [2–4]. AE hosts the discharge product of Li_2O_2 deposited during discharge and decomposes it during charge. The insulative aspect of the Li_2O_2 product involves large charging overvoltage, which causes oxidative degradation of the battery materials to deteriorate the battery performance along with the discharge/charge cycles. Metals and metal-oxide catalysts have been supported on AEs to decrease the charging overvoltage and improve the cycle life of LABs [5–9]. However, because such catalysts also promote the AE and electrolyte decomposition, whether they are beneficial for extending cycle life and overall battery performance remains controversial.

Alternatively, redox mediators (RMs) have been used to decrease charging overvoltage [10]. During charging, RM is oxidized to RM^+ ($RM \rightarrow RM^+ + e^-$) at the redox potential of RM (E_{redox}), and the generated RM^+ chemically oxidizes the Li_2O_2 to return to RM ($Li_2O_2 + 2RM^+ \rightarrow 2Li^+ + 2RM + O_2$), instead of the direct electrochemical oxidation of Li_2O_2 ($Li_2O_2 \rightarrow 2Li^+ + 2e^- + O_2$). The LAB with RMs can charge the cell near the E_{redox} without increasing the charging voltage indefinitely. RM is typically introduced in LAB cells by dissolving it in an electrolyte (RM-in-EL). However, this risks charging failure resulting from the “shuttle effect” [11]. The RM^+ generated at the E_{redox} during charging migrates to the Li metal anode to be

reduced without oxidizing the Li_2O_2 on AE. This migration provides a seemingly stable charging profile, but no appropriate charging is processed. RM can be incorporated on AE (RM-on-AE) to mitigate the shuttle effect. We have previously demonstrated that the LAB cell with LiBr-coated AE (LiBr-on-AE) extends the discharge/charge cycle life twice, in which the Br^- anion as inorganic RM was localized near AE to reduce the chance of shuttle effect, prolonging the RM effect throughout the discharge/charge cycles [12, 13]. Furthermore, LiBr-on-AE promotes the AE surface reduction of LiO_2, an intermediate of the ORR during discharge, to form the filmy low-crystalline discharge product of Li_2O_2 [13]. RM-on-AE has a synergistic effect on LAB, reducing the charging overvoltage by using the RM effect for a long duration and plating the Li_2O_2 deposit for easier decomposition.

Inorganic Li salts of LiI [14, 15], LiBr [16–18], $LiNO_3$ [19, 20], and $LiNO_2$ [21] have been investigated as RM, in which the dissociated anion functions as an RM agent. Inorganic RMs can be used in “RM-in-EL” and “RM-on-AE” conditions. However, there is a substantial concern regarding the corrosion of the base metals by the anions. Because halogen ions erode steel and copper used as current collectors and cell packaging [22], inorganic RM anions can result in battery leakage and disconnection during use or storage, in contrast to organic RMs. Organic molecules having their own redox potentials, porphyrins and phthalocyanines, including tetrathiafulvalene (TTF) [23, 24], 2,2,6,6-tetramethylpiperidine 1-oxyl (TEMPO) [25], and 10-methylphenothiazine (MPT) [26] (Figure 1), had been considered as organic RMs. Some organic molecules have quenching functions of active oxygen species by their non-localized π-conjugated and steric molecular structure [27–29], and therefore, organic RMs can be designed to provide high oxidative tolerance to electrolytes and carbon cathodes. However, organic RMs tend to be highly susceptible to reductive decomposition by Li metal anode, especially for “RM-in-EL,” in which the dissolved organic RMs are always in contact with

stripped Li metal anode. Several previous studies conducted discharge/charge experiments using a "dummy" anode, such as a $LiFePO_4$ electrode, in place of an Li anode, to avoid the reductive decomposition of RMs [23, 30]. However, these substituted anodes do not provide an accurate representation of the organic RM efficacy for LABs cycle operation. The "RM-on-AE" condition can solve the issue of the use of organic RMs, but there has been no report on the organic RM incorporation on AE to derive the RM effect well. The appropriate selection of organic RM species and optimization of their implementation into LABs remain a critical challenge.

This study maximizes the use of organic RMs by coating the three typical organic RMs—TTF, TEMPO, and MPT—on AE and investigating their LAB cell performance. TTF was first introduced as RM for LABs by Bruce et al., with a low charging voltage of 3.44 V [23]. TEMPO is a stable organic radical that can serve as RM with an E_{redox} of 3.76 V [25]. MPT has been recently reported as organic RM with remarkable electrochemical stability, repeating highly reversible redox at 3.68V [26]. The discharge/charge cycle test and the postmortem electrodes analysis revealed that the organic RM incorporation on AE (RM-on-AE) derives the RM effect well, rather than dissolving it in an electrolyte (RM-in-EL), by successfully suppressing the RM decomposition on the Li anode. Among the three organic RMs, the cell with MPT-on-AE exhibited the best cycling performance, resulting from the electrochemical stability of MPT and the reduced side reactions during the discharge/charge cycles. This study offers a practical design of RMs and their use in developing long-life LABs.

Experimental

Preparation of AEs

AE without RMs (RM-Free AE) was prepared by coating a slurry of Ketjen black (KB, EC600 JD, Lion Specialty Chemical) mixed with polyvinylidene fluoride/*N*-methylpyrrolidone solution (PVDF/NMP, 12 wt%, Kureha) on carbon paper (TGP-H-060, Toray) at a weight ratio of KB/PVDF = 9/1. The loaded amount of KB was adjusted to 1 mg cm^{-2}. For the preparation of RM-on-AE, the KB slurries dissolving TTF (Sigma-Aldrich, 97%), TEMPO (Sigma-Aldrich, 98%), or MPT (Sigma-Aldrich, 98%) were coated on the carbon paper with the KB loading of 1 mg cm^{-2}. The loaded amount of RM (TTF, TEMPO, or MPT) on AE was adjusted to 2 μmol cm^{-2}, corresponding to the molar amount of 50 mM RM concentration once it was dissolved in 80 μL electrolyte filled in a cell.

Cell assembly and battery testing

Lithium nitrate ($LiNO_3$, 99.99%, Sigma-Aldrich) was dissolved in tetraethylene glycol dimethylether (TEG, Nippon Emulsifier Co., Ltd.) at a concentration of 1 M as LAB electrolyte in this study (1 M $LiNO_3$/TEG). The LAB cell was assembled in an Ar-filled glove box by comprising a layer of a lithium metal foil anode (0.5 mm thick, Honjo Metal), a glass microfiber separator (GF/A, Whatman), and an AE, in a size of ϕ16 mm (2.0 cm^2 electrode area) inside a gastight cell chamber with gas inlet/outlet valves. The separator and AE were immersed in 80 μL of electrolyte before the battery testing. The discharge/charge cycle test was conducted in current constant mode at 0.2 mA cm^{-2} for 2.5 h with a cycle capacity of 0.5 mAh cm^{-2} (500 mAh g^{-1} per KB cathode weight) with discharge/charge cutoff voltages of 2.0/4.5 V at 25ºC. Pure oxygen gas was continuously supplied to the gastight cell chamber. For cyclic voltammetry (CV) measurement, a glassy carbon disk, Pt wire, and Ag | 0.1 M $AgNO_3$ + 1 M

$LiNO_3$/TEG were used as working, counter, and reference electrodes. The electrodes were immersed in a solution of 1 M $LiNO_3$/TEG containing 50 mM RM. Voltage sweeps were conducted under an Ar atmosphere in a range of 2.0–4.5 V vs. Li/Li^+ at a rate of 100 mV s^{-1}.

Electrodes analysis

After the discharge/charge cycle test, AEs and Li foil anodes were taken out from the cell chamber and rinsed with pure TEG solvent several times in an Ar-filled glove box to be observed and analyzed by scanning electron microscopy (SEM, JSM-7800F, JEOL) and energy dispersive X-ray spectroscopy (EDS, X-MAX^N, Oxford) equipped with the SEM. For quantifying the Li_2O_2 discharge product on AE, the AE (after the cycle test) was placed in a vessel containing a solution of 2wt% $TiOSO_4$ in 1.0 M H_2SO_4 to produce the equimolar amount of $[Ti(O_2)]^{2+}$ from Li_2O_2 ($TiOSO_4 + Li_2O_2 \rightarrow [Ti(O_2)]^{2+} + SO_4^{2-} + Li_2O$) [31]. Li_2O_2 was quantified by correlating the UV-Vis absorbance (UV2600, Shimadzu Corp.) of $[Ti(O_2)]^{2+}$ at the wavelength of 410 nm with a calibration curve derived from the $[Ti(O_2)]^{2+}$ solutions of known concentrations.

The byproducts of the discharge/charge reaction of Li_2CO_3 and carboxylates (RCOOLi) on AEs were quantified according to the literature [32], briefly by converting each component to the equimolar amount of CO_2 gas to be quantified. The $LiCO_3$ on AEs was quantified by soaking the AE (after the discharge/charge test) in 0.5 mL of 0.1 M H_2SO_4 in a glass-sealed vial of known volume to release CO_2 gas based on the following reaction: $H_2SO_4 + Li_2CO_3 \rightarrow Li_2SO_4 + H_2O + CO_2$. RCOOLi was quantified by soaking AE in a 0.5 mL mixture solution of 0.5 M $FeSO_4$ in 0.1 M H_2SO_4 / 10wt% H_2O_2 in 0.1 M H_2SO_4 at a volume ratio of 10/3 (Fenton's reagent) in a glass sealed vial of known volume to release CO_2 gas based on the following reaction: $RCOOLi + 2H_2O_2 \rightarrow RLi + 2H_2O + O_2 + CO_2$. The CO_2 gas concentration

inside the glass-sealed vials was measured using gas chromatography (GC2030, Shimadzu Corp.) equipped with a Dielectric-Barrier Discharge Ionization Detector (BID) and a MICROPACKED ST packed column. Helium was used as a carrier gas.

Results and discussion

Electrochemical properties of organic RMs

CV measurements were performed with the 50 mM RM solutions dissolved in 1 M $LiNO_3$/TEG to examine the electrochemical properties of TTF, TEMPO, and MPT (Figure 1) in the TEG-based LAB electrolyte. Figure 2(a) illustrates the CV profiles, exhibiting on-set potentials for RM oxidation of 3.1, 3.5, and 3.7 V for TTF, TEMPO, and MPT. These on-set potentials satisfy the E_{redox} requirement as RM of LAB, which must be higher than the thermodynamic potential of lithium-air (2.96 V), as with the lowest possible voltage that enables low charging voltage to mitigate oxidative degradation of the battery materials. The lowest on-set potential of TTF suggests that the TTF molecule can provide the lowest charging voltage among the organic RMs used in this study. However, the magnified CV profile depicted in Figure 2(b) revealed that TTF in 1 M $LiNO_3$/TEG electrolyte tends to lose redox reversibility, with declining oxidation current according to the CV scans. In contrast, although the on-set potentials of TEMPO and MPT were higher than the TTF, they exactly traced their profiles for up to three cycle scans, suggesting that these molecules have better redox reversibility and would be more suitable as RMs. The CV profiles also revealed the best reductive tolerance of MPT. While the MPT electrolyte demonstrated a negligibly small reductive current in the LAB's discharge voltage range of 1.5–3.0 V, the TTF and TEMPO electrolytes allowed appreciable reduction currents in that voltage region, implying the considerable reductive decomposition occurs during the discharge for TTF- and TEMPO-

incorporated cells. This result infers the superiority of the MPT molecule among the organic RMs in this study, as discussed in the next section.

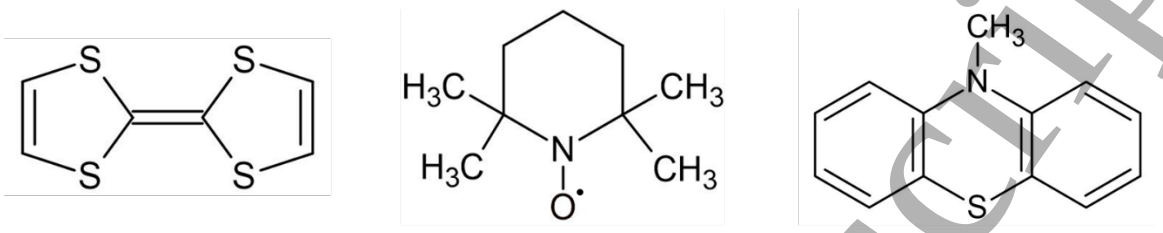

Tetrathiafulvalene (TTF) | 2,2,6,6-Tetramethylpiperidine 1-Oxyl (TEMPO) | 10-Methylphenothiazine (MPT)

Figure 1. Organic RMs investigated in this study.

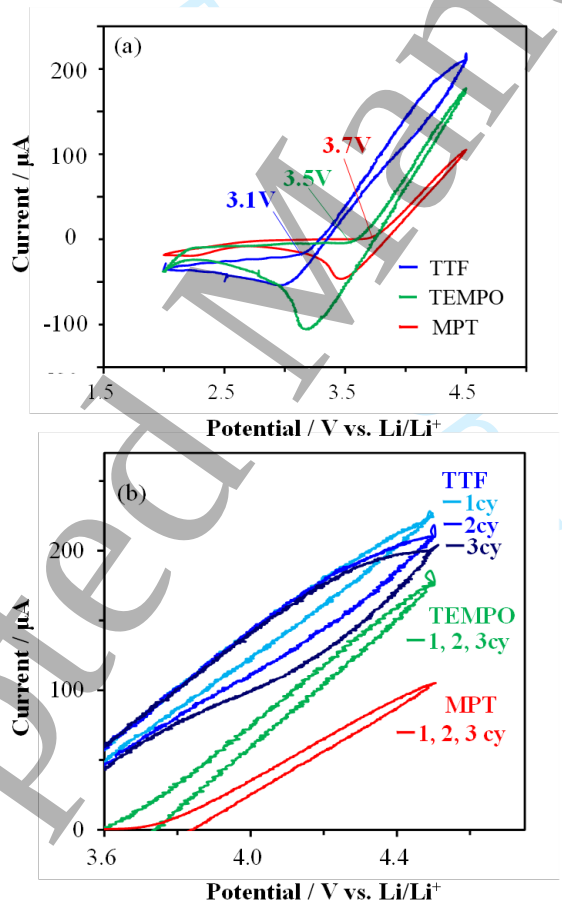

Figure 2. (a) CV curves of TTF (blue), TEMPO (green), and MPT (red) 50 mM solution in 1 M $LiNO_3$/TEG electrolyte. (b) Magnified CV curves in the potential region of 3.6–4.5V.

Battery performance

As mentioned previously, there are two methods of introducing RMs into LAB cells: RM-in-EL and RM-on-AE. Discharge/charge cycle tests of the LAB cells without RM (RM-Free) and with RM incorporated in the electrolyte (RM-in-EL) or coated on AE (RM-on-AE) were conducted to derive the RM effect of the organic RMs. Figure 3 illustrates the result of the cells in which MPT was used as organic RM, exhibiting the discharge/charge profiles (a-c) and midpoint voltages (d) of up to 15 cycle runs. After all cells exhibited a stable 2.6 V discharge voltage plateau up to the 10th discharge, the RM-Free cell experienced a rapid drop in the discharge voltage. Similarly, the RM-Free cell exhibited increasing charge voltage from the seventh charge, whereas the MPT-in-EL and MPT-on-AE cells maintained charge voltage plateaus of 3.5–3.7 V, corresponding to the E_{redox} of MPT. This result demonstrates that the MPT incorporation into LAB cell facilitates the Li_2O_2 decomposition during charging to mitigate the battery material deterioration and extend the cycle life. Figure 3(e) illustrates the dQ/dV curves derived from the charging profiles, confirming that the MPT-on-AE cell, with the lowest peak voltage of 3.45 V up to the 10th charge, has the most effective charging behavior. In contrast, the MPT-in-EL cell moved the peak position from 3.50 to 3.63 V at the 10th cycle charge. The cell with no MPT (RM-Free) exhibited a dQ/dV peak at 3.60 V for up to the fifth charge, which moved to 3.85 V at the 10th charge while decreasing in intensity. Consequently, the RM-Free cell rapidly loses its charging voltage control, immediately deteriorating cell performance. Incorporating MPT as RM improves cell voltage control, and its RM function is most effectively derived by introducing it on AE.

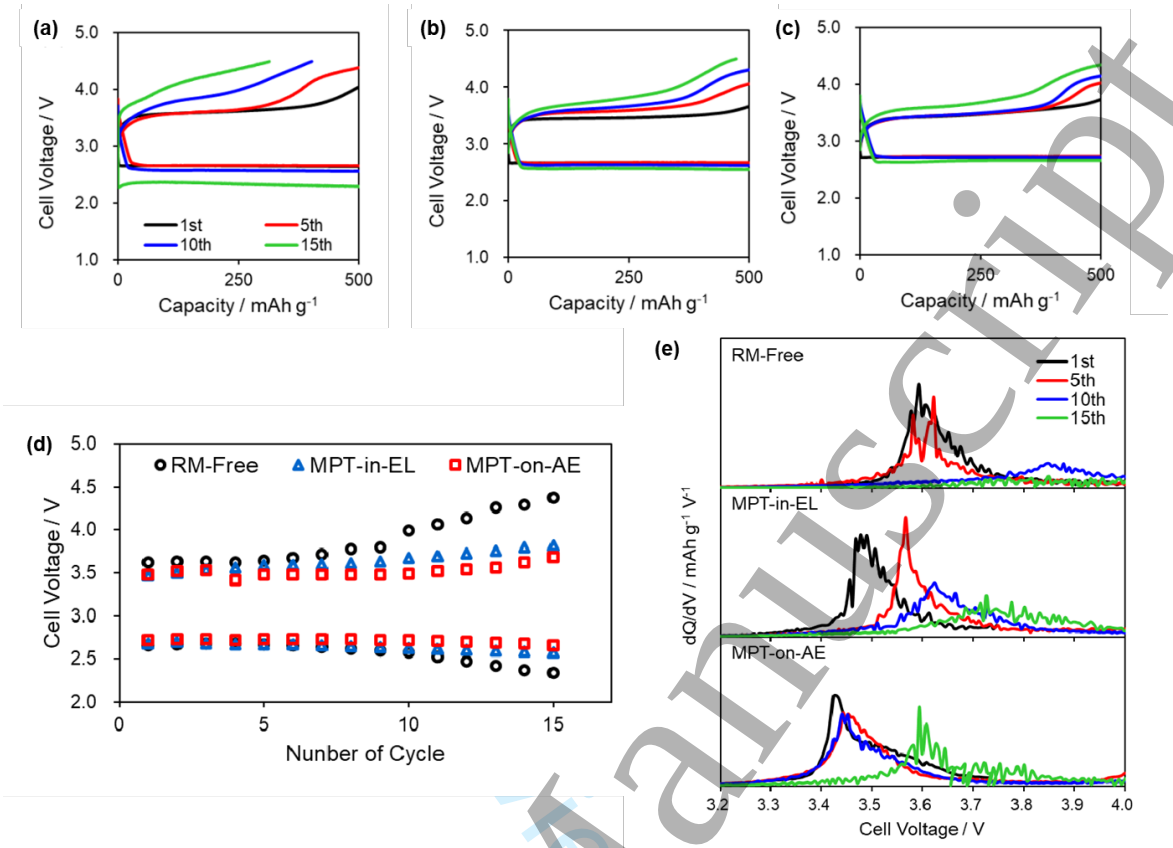

Figure 3. (a-c) Discharge/charge curves for RM-Free (a), MPT-in-EL (b), and MPT-on-AE (c) cells. (d) Midpoint cell voltages. Cell voltages at the 250 mA g^{-1} capacity were plotted against the cycle number. (e) dQ/dV curves derived from the charge profiles depicted in (a-c).

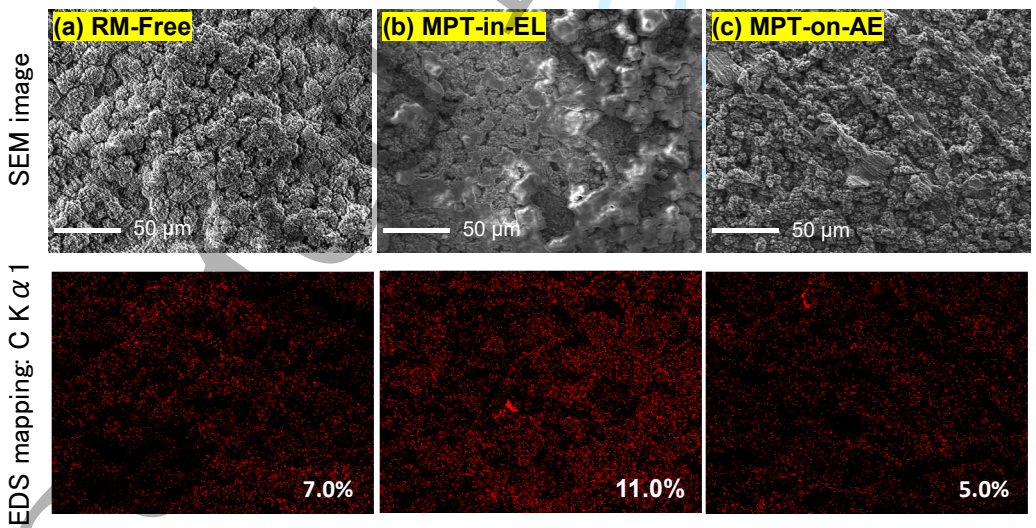

Figure 4. SEM images (up) and their C element mapping (bottom) of Li metal anodes after one discharge-charge cycle of RM-Free (a), MPT-in-EL (b), and MPT-on-AE (c) cells. The number in the C mapping is the atomic element ratio of carbon.

Figure 4 illustrates the SEM images of the lithium metal anodes after one discharge/charge cycle. The dissolution and deposition of lithium by the discharge/charge gave the granular shape deposits on the anode surfaces in the $LiNO_3$/TEG electrolyte rather than forming needle-like dendritic morphology [33, 34]. The surface morphologies for RM-Free and MPT-on-AE cells were almost similar, while the MPT-in-EL exhibited smear deposits on the granular surface. The EDS elemental analysis revealed exceptionally high carbon (C) element deposition (11% atom) on the anode of the MPT-in-EL cell. This high deposition indicates that MPT undergoes reductive decomposition by directly contacting lithium metal to produce an insulative product on the anode. However, this was suppressed when the MPT was incorporated on AE rather than EL, explaining the prolonged RM effect of the RM of MPT for the MPT-on-AE cell. Even though, because the MPT molecules were only impregnated in AE in soluble form here, there is a possibility of MPT leaching into the electrolyte during long-term storage or cycling experiment, where the MPT-on-AE and MPT-in-EL cells may eventually lead to same performance. To prevent the RM dissolution from AE, physical or chemical anchoring of RM on the cathode surface would be inevitable in the future, as reported in previous literature [35, 36].

On the basis of successfully incorporating MPT-on-AE as organic RM, the discharge/charge cycle tests were also conducted for the cells with TTF-on-AE, TEMPO-on-AE, and MPT-on-AE. Figure 5 illustrates the resulting discharge/charge curves of up to 20 cycles (a)–(c) and their midpoint cell voltages (d). Even though the lowest on-set potential of TTF, the TTF-on-AE cell demonstrated the most unstable cycling behavior, exhibiting a rapid increase in the discharge/charge overpotentials to lose the cell voltage control after the 15th cycle caused by the electrochemical deactivation of the TTF molecules during the cycle, as indicated in the CV behavior in Figure 2(b). In contrast, the TEMPO-on-AE and MPT-on-AE cells exhibited stable discharge/charge behavior up to their 20th cycle runs. In comparing the

TEMPO-on-AE and MPT-on-AE cells, the MPT-on-AE cell most successfully suppresses the discharge/charge overpotentials and maintains battery performance for higher cycle numbers.

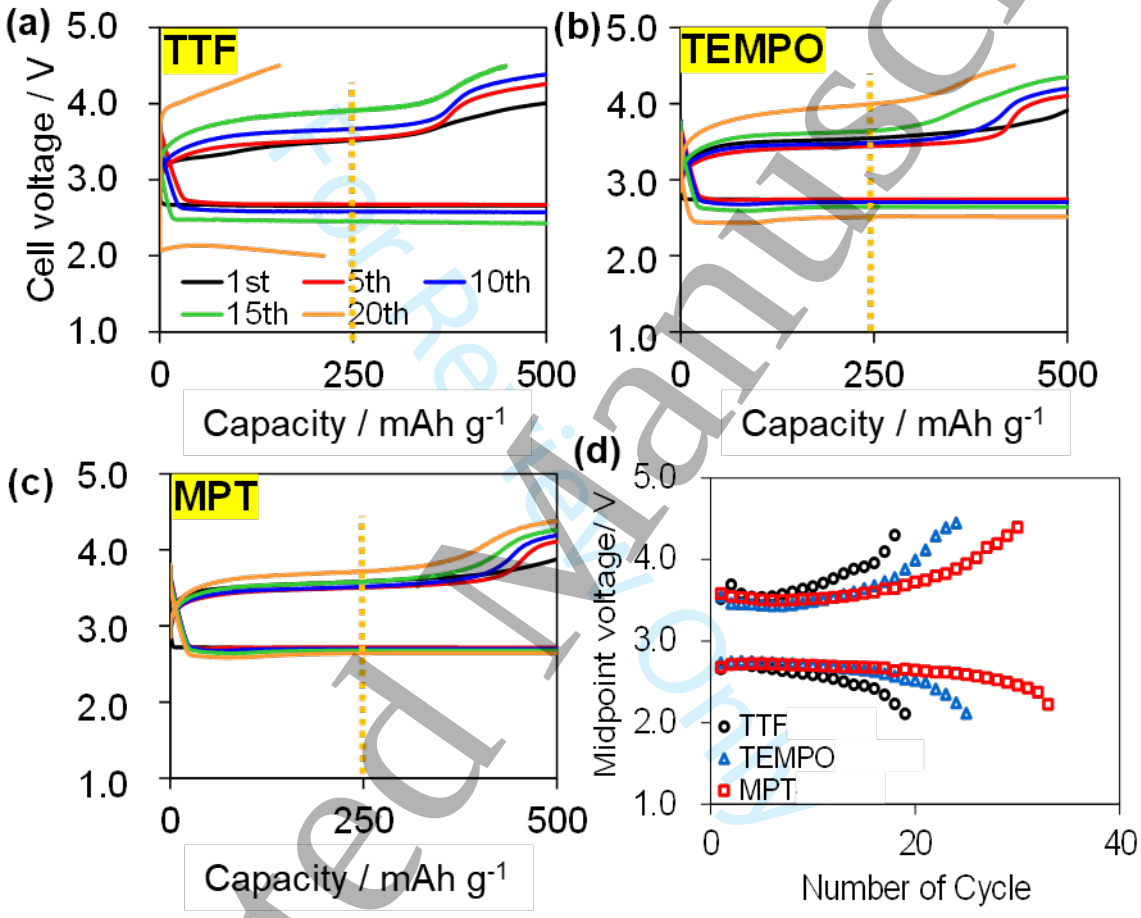

Figure 5. (a-c) Discharge/charge curves of TTF-on-AE (a), TEMPO-on-AE (b), and MPT-on-AE (c) cells. (d) Midpoint cell voltages. Cell voltages at the 250 mA g^{-1} capacity were plotted against the cycle number.

Postmortem analysis of the electrodes was conducted to examine the battery performance of the RM-on-AE cells. Figure 6 illustrates the SEM images of the Li metal anode surfaces from the RM-Free (a), TTF-on-AE (b), TEMPO-on-AE (c), and MPT-on-AE (d) cells after one discharge/charge cycle. Compared with the surface morphology of RM-Free with a granular deposit (a), there was no significant morphological difference in the RM-on-AE cells (b-d), suggesting that lithium metal was deposited correctly on the anode after all cells were charged. However, the EDS elemental analysis of the anode surface revealed that the anode from the TTF-on-AE cell had a higher element ratio of C (21%) than other cells (5%–9%). Thus, TTF is more likely to be decomposed during the discharge/charge and deposit the degradant on the anode, even though the molecule was supported on AE. The structural optimization based on first principles using Gaussian 16W software revealed that the C-S bond in each RM molecule is about 1.7 Å, which is longer than the other C-C, C=C, and C-N bond distances of 1.3–1.5 Å (supplemental information). Consequently, the TTF molecule with four C-S bonds is more likely to undergo side reactions than TEMPO and MPT. In contrast, the anodes from TEMPO-on-AE and MPT-on-AE cells provided similar elemental distribution with the RM-Free cell, suggesting fewer such side reactions. The TTF molecule is likely unsuitable as an organic RM because of the significant side reactions that degrade battery performance more quickly.

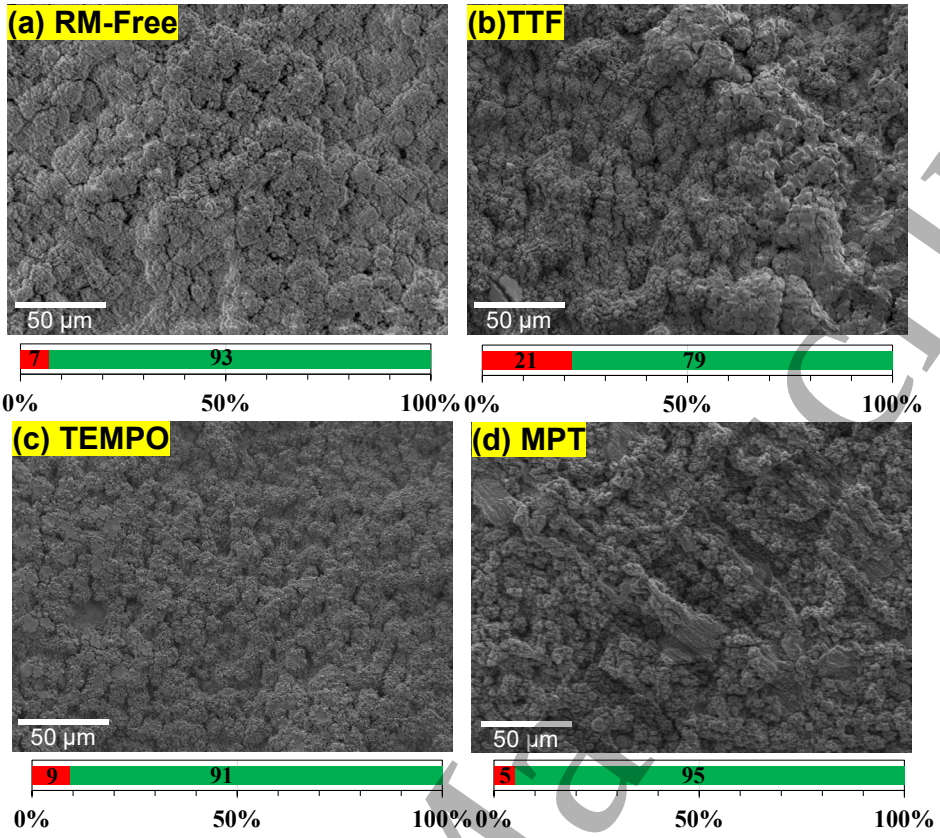

Figure 6. SEM images of lithium metal anodes from RM-Free (a), TTF-on-AE (b), TEMPO-on-AE (c), and MPT-on-AE cells after the one discharge/charge cycle. The bar graph at the bottom of each image represents the elemental component ratio of carbon (C, red) and oxygen (O, green).

SEM observations were also conducted for the AEs after the discharge/charge cycle test. Figure 7 illustrates the SEM images of AEs from TEMPO-on-AE cells (a, b), and MPT-on-AE cells (c, d) after the 10th discharge (10Dc, a, c) and the 10th charge (10Ch, b, d), as with the corresponding oxygen (O) element mapping. The AE from the TEMPO-on-AE cell hosted filmy Li_2O_2 with no particular shape particles after discharge, which was accordingly decomposed by charging with reducing the O element ratio. In contrast, the AE from MPT-on-AE cells deposited toroidal Li_2O_2 particles of several micrometer diameters (the magnified image depicted in (e)), which was well decomposed by the charging, leaving no particles. The morphological difference in the discharge product characterizes the two different ORR

pathways: “surface reduction” and “disproportionation” reactions [37]. LiO_2, a one-electron reduction product of ORR intermediate ($O_2 + e^- + Li^+ \rightarrow LiO_2$), is further reduced to be Li_2O_2 by adopting one more electron from AE surface ($LiO_2 + e^- + Li^+ \rightarrow Li_2O_2$) or undergoes the disproportionation to precipitate the crystalline particles of Li_2O_2 ($2LiO_2 \rightarrow Li_2O_2 + O_2$). The filmy deposit on TEMPO-on-AE exemplifies the Li_2O_2 deposit from the surface reduction process, while the toroid particles on MPT-on-AE represent the deposit by the disproportionation pathway. Condensed π structure of the TEMPO molecule can promote surface isomorphic growth of Li_2O_2, as reported by Wang et al [35], which would have changed the particle Li_2O_2 geometry to the thin film deposit for TEMPO-on-AE. Furthermore, TEMPO-on-AE generated less Li_2O_2 than the quantitative cycle capacity, as discussed in the next section, explaining the negligible Li_2O_2 particles deposited on TEMPO-on-AE. MPT-on-AE hosts and decomposes Li_2O_2 particles to secure the AE pores for ORR, producing the best discharge/charge cycle performance in the LAB cells.

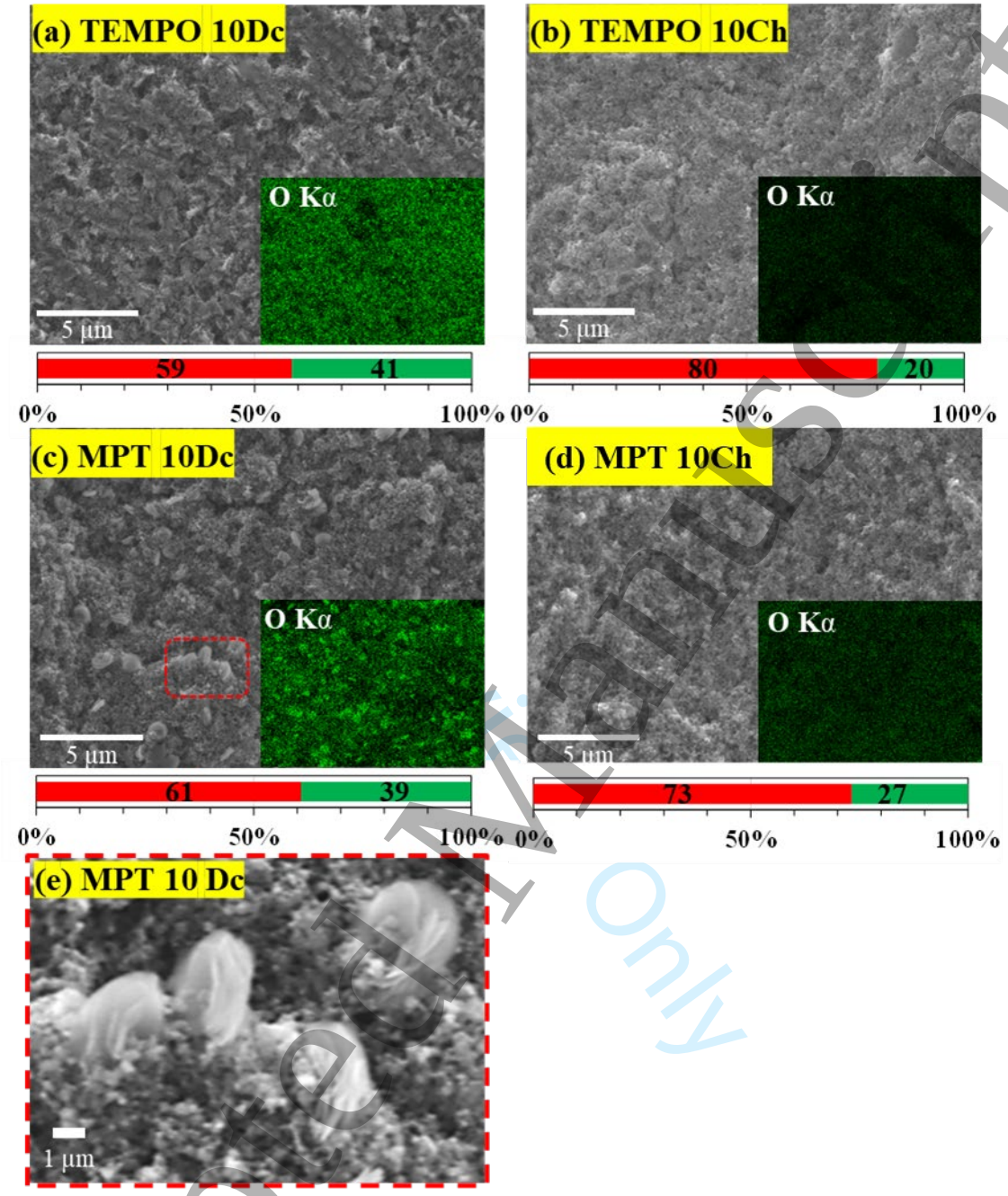

Figure 7. SEM images of AEs from TEMPO-on-AE (a, b) and MPT-on-AE (c, d) cells after the 10th discharge (a, c) and 10th charge (b, d). The bar graph at the bottom of each image illustrates the elemental component ratio of carbon (C, red) and oxygen (O, green). (e) Magnified image of the red dotted square in (c).

Quantitative analysis of precipitates on AEs

The amount of Li_2O_2 on AEs was determined by colorimetric titration to evaluate the discharge product deposition/decomposition efficiency. Figure 8 summarizes the result, in which the dotted line represents the quantitative amount of Li_2O_2 by the ideal ORR of the cycle capacity (18.65 μmol for 1.0 mAh discharge). For all cells, the generated amount of Li_2O_2 by discharge (Dc) was less than the theoretical amount, and the Li_2O_2 could not be fully decomposed by charge (Ch), representing the overall limitation on the reversibility of present LAB technology. The graph revealed that the cells with TTF-on-AE and TEMPO-on-AE generate no more than 60% of Li_2O_2 of the theoretical amount after first discharge (1Dc), while the RM-Free and MPT-on-AE cells produce 96% of the theoretical amount after 1Dc. Thus, significant irrelevant side reactions occurred with the TTF-on-AE and TEMPO-on-AE cells, confirming the incompatibility of these molecules as RMs of LABs. Given the considerable reductions demonstrated for the TTF and TEMP electrolytes (Figure 2(a)), TTF-on-AE and TEMPO-on-AE should have consumed the most electrons for their molecule reductions instead of generating Li_2O_2. This phenomenon might have been accentuated for the RM-on-AE case, in which the TTF and TEMPO molecules are localized near the AEs to interfere with the ORR process. The structural optimization calculation revealed the higher LUMO energy of MPT than the LUMO of TTF and the singly occupied molecular orbital (SOMO) of TEMPO (supplemental information), which suggests the high reductive stability of the MPT molecule during the discharge. Figure 8 also revealed that RM-Free cells fail to decompose Li_2O_2 by charging, leaving a substantial amount of Li_2O_2 on AE after the charge (1Ch, 10Ch, and 20Ch). However, the MPT-on-AE cell decomposes the Li_2O_2 well by charging, providing the best rechargeable ability among the LAB cells investigated in this study, despite the Li_2O_2 generation efficiency declining to 57% for its 20th discharge (20Dc).

This result suggests that further development of battery materials with oxidative stability is necessary to establish long-life LABs.

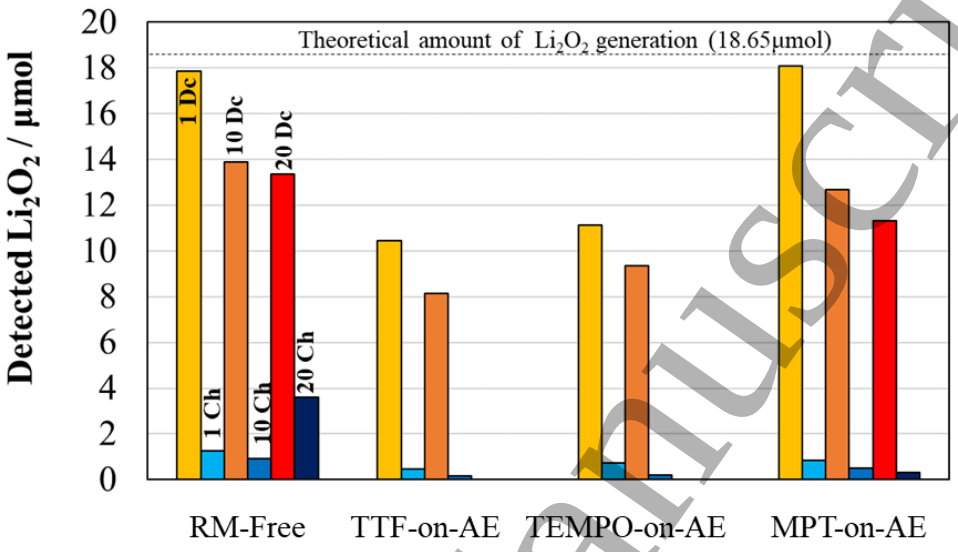

Figure 8. Detected Li_2O_2 amount on AEs after discharge/charge cycle test. The dotted line represents the theoretical Li_2O_2 amount of 18.65 μmol for a cell capacity of 1.0 mAh (0.5 mAh cm^{-2}, 500 mAh g^{-1}). The notations of 1Dc, 1Ch, 10Dc, 10Ch, 20Dc, and 20Ch denote the AEs from the cells after the first discharge, first charge, 10th discharge, 10th charge, 20th discharge, and 20th charge.

In addition to the Li_2O_2 deposit on AEs, Li_2CO_3, and carboxylates (RCOOLi) on AEs, which are significant byproducts resulting from oxidative degradation of electrolytes or AE carbons [38], were quantified. Figure 9 reveals that Li_2CO_3 (a) accumulates on AEs along with discharge/charge cycles for all cells. Furthermore, several micromolar amounts of carboxylates were generated from the first discharge and charge. The carboxylates were not accumulated along with cycles, indicating that this chemical species is produced and then further oxidized to Li_2CO_3 to be accumulated on AE, or to CO_2 and H_2O to be released from the cell [39]. After the 10th charge, the accumulated amount of Li_2CO_3 on AEs reaches 5.2–8.3 μmol, corresponding to 28%–45% of the molar amount of ideal Li_2O_2

deposition/decomposition (18.65 μmol). Battery performance deterioration and cell death occur with these byproduct depositions and accumulations, and therefore it is necessary to prevent the side reactions from the very first discharge and charge. The graph indicates that the MPT-on-AE cells most successfully suppress the Li_2CO_3 and carboxylates generation from the first discharge and charge, resulting from the superior RM effect of MPT, despite molar amounts of Li_2CO_3 and carboxylates on MTP-on-AE after the first charge of 0.6 and 0.4 μmol, corresponding to 3.2% and 2.1% of the theoretical amount of Li_2O_2 deposition/decomposition. Consequently, some percent of electrons are still consumed for the irrelevant side reactions, even in the cell with MPT-on-AE. The result requires further exploration of electrolytes and electrodes with oxidative tolerance against active oxygen species. This study provides insight into developing the battery materials of long-life LABs using organic RMs.

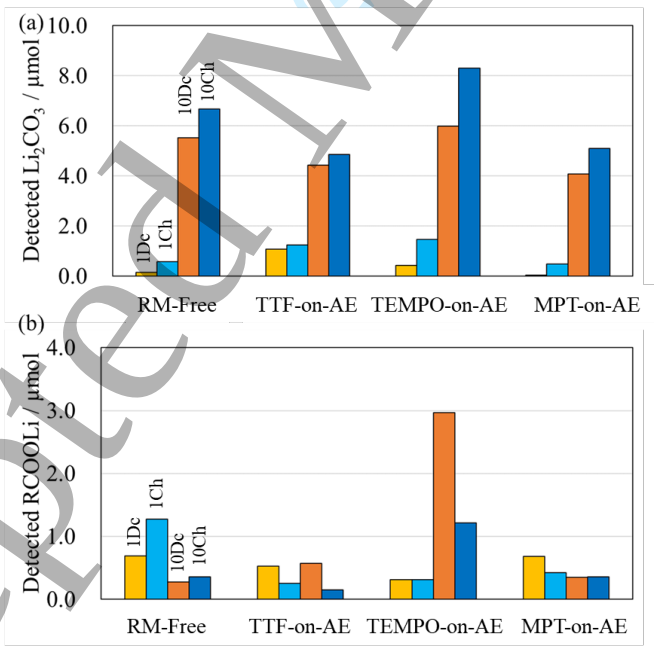

Figure 9. Detected amount of Li_2CO_3 (a) and carboxylates (RCOOLi, b) on AE after discharge/charge cycle test.

Conclusions

RMs reduce charging voltage to improve the energy efficiency and cycle life of LAB cells. However, the shuttle effect and reductive decomposition of organic RMs can adversely deteriorate cell performance. This study demonstrated the successful implementation of organic RMs by the RM-on-AE method, in which the RMs are localized near the AE surface to avoid the reductive decomposition and shuttle effect and thus prolong the RM effect throughout the discharge/charge cycle lives. This result supports our previous studies on the LABs with inorganic RMs [13], demonstrating the potential of organic RMs that can be well-designed to grant high oxidative stability against active oxygen species. Of the organic RMs TTF, TEMPO, and MPT, the MPT-on-AE cells demonstrated the best discharge/charge cycle performance, resulting from the molecular structure of MPT providing excellent redox reversibility as with the reductive tolerance in the voltage window of LABs. The further design of organic RMs will produce a breakthrough that will fundamentally improve the life cycle of LABs. This study provides the pivotal design of organic RMs and their appropriate implementation in LABs.

Acknowledgments

This work was partly supported by the Japan Science and Technology Agency (JST) via the Specially Promoted Research in Next Generation Batteries Area in Advanced Low Carbon Technology Research and Development Program (ALCA-SPRING, grant no. JPMJAL1301) by the National Institute for Materials Science (NIMS) Joint Research Hub Program. Materials and cell assembly were characterized at the NIMS Battery Research Platform. The authors are grateful to the Battery Research Platform of the NIMS for providing experimental facilities. The authors declare no competing interests.

References

1. W. J. Kwak, Rosy, D. Sharon, C. Xia, H. Kim, L. R. Johnson, P. G. Bruce, L. F. Nazar, Y. K. Sun, A. A. Frimer, M. Noked, S. A. Freunberger and D. Aurbach, *Chem. Rev.*, **120**, 6626 (2020).

2. A. Nomura, E. Mizuki, K. Ito, Y. Kubo, T. Yamagishi and M. Uejima, *Electrochim. Acta*, **400** (2021).

3. K. Ushijima, S. Iwamura and S. R. Mukai, *ACS Appl. Energ. Mater.*, **3**, 6915 (2020).

4. Y. Lin, B. Moitoso, C. Martinez-Martinez, E. D. Walsh, S. D. Lacey, J. W. Kim, L. M. Dai, L. B. Hu and J. W. Connell, *Nano Lett.*, **17**, 3252 (2017).

5. F. Li, D.-M. Tang, Y. Chen, D. Golberg, H. Kitaura, T. Zhang, A. Yamada and H. Zhou, *Nano Lett.*, **13**, 4702 (2013).

6. Y.-C. Lu, Z. Xu, H. A. Gasteiger, S. Chen, K. Hamad-Schifferli and Y. Shao-Horn, *J. Am. Chem. Soc.*, **132**, 12170 (2010).

7. Y. Yu, B. Zhang, Y.-B. He, Z.-D. Huang, S.-W. Oh and J.-K. Kim, *J. Mater. Chem. A*, **1**,

1163 (2013).

8. R. Black, J.-H. Lee, B. Adams, C. A. Mims and L. F. Nazar, *Angewandte Chemie International Edition*, **52**, 392 (2013).

9. J.-J. Xu, D. Xu, Z.-L. Wang, H.-G. Wang, L.-L. Zhang and X.-B. Zhang, *Angewandte Chemie International Edition*, **52**, 3887 (2013).

10. J. B. Park, S. H. Lee, H. G. Jung, D. Aurbach and Y. K. Sun, *Adv. Mater.*, **30** (2018).

11. P. G. Bruce, S. A. Freunberger, L. J. Hardwick and J. M. Tarascon, *Nature materials*, **11**, 19 (2012).

12. Y. Hayashi, R. Honda, I. Moro, M. Fukunishi, H. Otsuka, Y. Kubo, T. Horiba and M. Saito, *Electrochemistry*, **89**, 557 (2021).

13. S. Azuma, M. Sano, I. Moro, F. Ozawa, M. Saito and A. Nomura, *The Journal of Physical Chemistry C*, **127**, 7087 (2023).

14. W. Zhang, Y. Shen, D. Sun, Z. Huang, J. Zhou, H. Yan and Y. Huang, *Nano Energy*, **30**, 43 (2016).

15. Y. Lin, C. Martinez-Martinez, J. W. Kim and J. W. Connell, *J. Electrochem. Soc.*, **167** (2020).

16. Z. J. Liang and Y. C. Lu, *J. Am. Chem. Soc.*, **138**, 7574 (2016).

17. X. Xin, K. Ito and Y. Kubo, *ACS Appl Mater Interfaces*, **9**, 25976 (2017).

18. K. Ito, D. Matsumura, C. Song and Y. Kubo, *ACS Energy Letters*, **7**, 2024 (2022).

19. D. Sharon, D. Hirsberg, M. Afri, F. Chesneau, R. Lavi, A. A. Frimer, Y.-K. Sun and D. Aurbach, *ACS Appl. Mater. Interfaces*, **7**, 16590 (2015).

20. Y. Hayashi, S. Yamada, T. Ishikawa, Y. Takamuki, M. Sohmiya, H. Otsuska, K. Ito, Y. Kubo and M. Saito, *J. Electrochem. Soc.*, **167**, 020542 (2020).

21. S. Azuma, M. Sano, I. Moro, F. Ozawa, M. Saito and A. Nomura, *Electrochim. Acta*,

489, 144261 (2024).

22. K. Schwabe and C. Voigt, *Electrochim. Acta*, **14**, 853 (1969).

23. Y. Chen, S. A. Freunberger, Z. Peng, O. Fontaine and P. G. Bruce, *Nat. Chem.*, **5**, 489 (2013).

24. W. R. Torres, S. E. Herrera, A. Y. Tesio, M. d. Pozo and E. J. Calvo, *Electrochim. Acta*, **182**, 1118 (2015).

25. B. J. Bergner, A. Schürmann, K. Peppler, A. Garsuch and J. Janek, *J. Am. Chem. Soc.*, **136**, 15054 (2014).

26. N. Feng, X. Mu, X. Zhang, P. He and H. Zhou, *ACS Appl. Mater. Interfaces*, **9**, 3733 (2017).

27. W. Miki, *Pure and Applied Chemistry*, **63**, 141 (1991).

28. N. Mahne, B. Schafzahl, C. Leypold, M. Leypold, S. Grumm, A. Leitgeb, Gernot A. Strohmeier, M. Wilkening, O. Fontaine, D. Kramer, C. Slugovc, Sergey M. Borisov and Stefan A. Freunberger, *Nature Energy*, **2**, 17036 (2017).

29. Y. K. Petit, C. Leypold, N. Mahne, E. Mourad, L. Schafzahl, C. Slugovc, S. M. Borisov and S. A. Freunberger, *Angewandte Chemie International Edition*, **58**, 6535 (2019).

30. X. Gao, Y. Chen, L. Johnson and P. G. Bruce, *Nature materials*, **15**, 918 (2016).

31. A. Dutta, K. Ito, A. Nomura and Y. Kubo, *Adv. Sci.*, **7** (2020).

32. M. M. Ottakam Thotiyl, S. A. Freunberger, Z. Peng and P. G. Bruce, *J. Am. Chem. Soc.*, **135**, 494 (2013).

33. F. Ozawa, K. Koyama, D. Iwasaki, S. Azuma, A. Nomura and M. Saito, *Electrochemistry*, **92**, 047003 (2024).

34. A. Dutta, K. Matsushita and Y. Kubo, *Adv. Sci.*, **n/a**, 2404245 (2024).

35. Y. Wang, L. N. Song, Y. F. Wang, F. Li, X. X. Wang, H. F. Wang and J. J. Xu, *Energy*

Storage Materials, **45**, 191 (2022).

36. Y. Ko, H. Park, K. Lee, S. J. Kim, H. Park, Y. Bae, J. Kim, S. Y. Park, J. E. Kwon and K. Kang, *Angew. Chem.-Int. Edit.*, **59**, 5376 (2020).

37. N. B. Aetukuri, B. D. McCloskey, J. M. Garcia, L. E. Krupp, V. Viswanathan and A. C. Luntz, *Nat. Chem.*, **7**, 50 (2015).

38. S. A. Freunberger, Y. H. Chen, N. E. Drewett, L. J. Hardwick, F. Barde and P. G. Bruce, *Angew. Chem.-Int. Edit.*, **50**, 8609 (2011).

39. A. Nomura, K. Ito, D. Y. W. Yu and Y. Kubo, *J. Power Sources*, **592**, 233924 (2024).